CHAPTER 7 Photoluminescence: Nitrogen-Vacancy and Silicon-Vacancy color centers

François Treussart, Igor Vlasov

CHAPTER 7
Photoluminescence: Nitrogen-Vacancy and Silicon-Vacancy color centers

François TREUSSART[†,*] **and Igor VLASOV**[‡]

[†]*Université Paris-Saclay, ENS Paris-Saclay, CNRS, LAC, 91405Orsay, France*
[‡]*A. M. Prokhorov General Physics Institute, Russian Academy of Sciences, 119991 Moscow, Russia*
[*]*Email : francois.treussart@ens-paris-saclay.fr*

NON-PRINT ITEMS Abstract Owing to its large bandgap of 5.5 eV, diamond can host a large variety of optically active defects (color centers). The most developed ones are two defects comprising in their structure an impurity atom (nitrogen or silicon), a vacant lattice site, and a trapped electron. These color centers are denoted as NV^- and SiV^-. Modern views about the structure of these defects are given in this Chapter. It is illustrated how NV^- spin is initialized and read-out at room temperature by means of Optically Detected Magnetic Resonance, leading to appealing applications, such as spin qubits and spin sensors. State-of-the-art and challenges of NV^- and SiV^- productions in nanodiamond are discussed. Some aspects of excitation modalities, photophysical parameters, detection techniques with ultra-high resolution, as well as biological applications of these two centers are addressed in this Chapter.

Key Words
Nitrogen-Vacancy; Silicon-Vacancy; Optically Detected Magnetic Resonance; Photoluminescence; Cathodoluminescence; Stimulated Emission Depletion; Fluorescent Marker

7.1 The Nitrogen-Vacancy color center

In high-pressure high temperature (HPHT) synthesis of diamond, as well as in detonation production method, Nitrogen (N) happens to be the most abundant impurity, sitting in substitution of carbon atoms. In type 1b diamond, nitrogen atoms are present as isolated impurities in the diamond lattice[1]. Under blue or green light excitation of such material, there is a photoluminescence (PL) in the red and near infrared spectral domains (**Figure 1d**), with characteristic narrow lines at 637 nm (**Figure 2b**) and 575 nm (**Figure 3b**), followed at higher wavelengths with a broad band. These spectral signatures are more pronounced in diamond that has been exposed to a high energy particle beam (**Figure 1e**), which is capable of displacing carbon atoms and leave a vacancy (V) behind, and even more intense after high temperature (≈800°C) annealing (**Figure 1f**).

These defects were therefore suspected from 1965 by Du Preez[2] to involve both nitrogen impurities and vacancies. The trigonal symmetry of the 637 nm emitting color center was then inferred from photoluminescence and uniaxial stress studies confirming that the defect must originate from a NV pair with the nitrogen-vacancy axis direction along the [111] diamond crystalline axis[3,4]. One year after, using electron paramagnetic resonance (EPR) under light excitation, Loubser and van Wyk observed in an irradiated and annealed diamond sample an EPR triplet signature that they attributed to the negative charge state (NV^-)[5,6]. In photoluminescence NV^- is the defect responsible for the 637 nm narrow line (1.945 eV in energy)[4], which is the zero-phonon line (ZPL) corresponding to the deexcitation of the excited NV^- center from the lowest energy vibrational level of the excited state to the lowest vibrational level of the ground state. The defect with the ZPL centered on 575 nm (2.156 eV) was attributed to the neutral state NV^0 by Mita[7] in 1996. Both NV^- and NV^0 have a PL that extends from the ZPL to higher wavelength due to vibronic phonon sidebands (**Figure 2** and **Figure 3**). The sharp ZPLs of the nitrogen vacancy indicate that they are deep-level defects in the diamond energy bandgap.

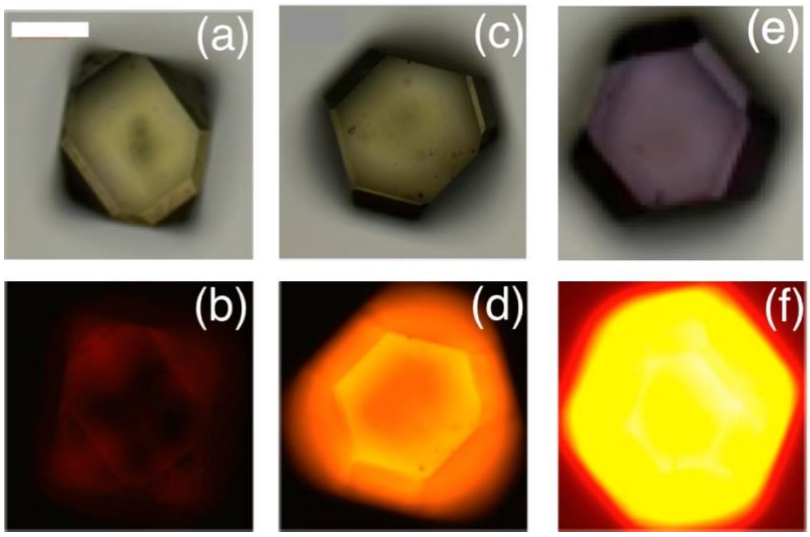

Figure 1 – Creation of NV color center in high pressure high temperature synthetic diamond microcrystals. (a),(c) and (e) White light illumination optical microscopy image of a diamond microcrystal at different stages of NV center creation process: as-received Micron+ MDA 0.1 (Element6 Ltd, England) microcrystals (a), microdiamond irradiated with a 8 MeV energy electron beam, at fluence of 2.10^{18} electrons/cm^2 but not annealed, and (c) irradiated and high temperature annealed (800°C, 2 hours, under vacuum) microcystal. (d) (resp. (e) and (f)) Same microcrystal than in (a) ((b) and (c) resp.) observed in epifluorescence microscopy. Epifluorescence images were acquired in identical conditions: excitation band wavelength 500-550 nm, detection with a longpass filter at wavelengths above 600 nm, and CCD array detector integration time of 1.5 s. The annealing induces the micrgration of the vacancies leading to the formation of a high concentration of NV center, which photoluminescence saturates the CCD array. Scale bar: 50 µm.

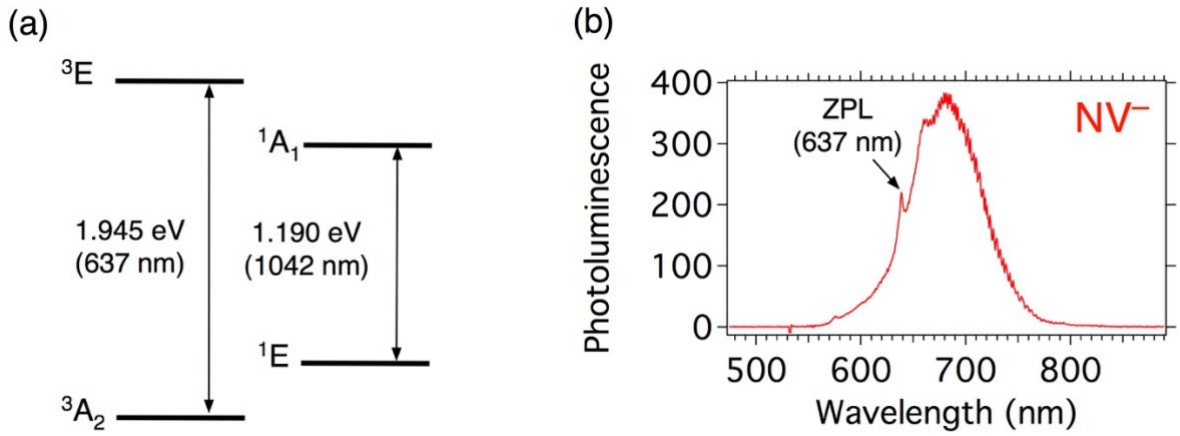

Figure 2 – Simplified electronic structure of negatively charge NV$^-$ and associated photoluminescence. (a) NV$^-$ simplified electronic structure showing the triplet $^3A_2$-^3E system, the singlet ^1E-$^1A_1$ metastable states and the energy associated to the zero-phonon lines of each system of levels. (b) Photoluminescence spectrum of a single NV$^-$ center at room temperature, under laser excitation at wavelength of 532 nm. The ZPL appears as a narrow line at wavelength 637 nm (energy 1.945 eV), and the phonon replica as a broad band at higher wavelengths.

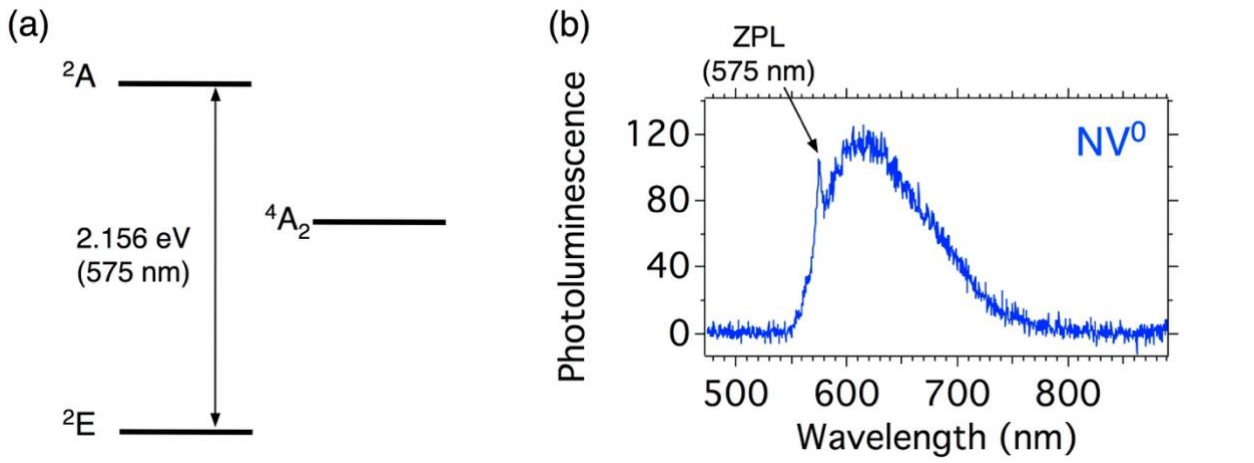

Figure 3 – Simplified electronic structure of neutral NV^0 and associated photoluminescence. (a) NV^0 simplified electronic structure showing the doublet ^{2}E-^{2}A system, the ^{4}A$_2$ metastable state and the energy associated to ^{2}E-^{2}A zero-phonon line. (b) Photoluminescence spectrum of a single NV^0 center at room temperature, under laser excitation at wavelength of 532 nm. The ZPL appears as a narrow line at wavelength 575 nm (energy 2.156 eV), and the phonon replica as a broad band at higher wavelengths.

NV center electronic structure at room temperature (simplified presentation)

Researches on NV center electronic structure are still very active because contradictory results have been obtained by different approaches and a full understanding of NV$^-$ most remarkable properties, *i.e.* the spin polarization by bight, is still lacking. An in-depth recent review of the NV center properties is presented in Doherty *et al.*[8]. A molecular model of NV$^-$ providing a complete electronic solution is also presented in Doherty *et al*.[9] Briefly, for NV$^-$, the calculation is based on (i) the NV center C_{3v} point group symmetry, and (ii) a model involving six electrons[5], five of them being electrons unpaired between the vacancy, the three nearest carbon atoms and the nitrogen atom, plus an additional electron trapped at the defect center. This even number of electrons is associated to an integer spin value. The center electronic state can then be described by configurations of molecular orbitals constructed according to group theory rules[10], as linear combinations of sp^3 orbitals of the vacancy nearest carbon and nitrogen atoms (see a full development of NV$^-$ molecular model in M. Doherty *et al.*[9]). These combinations include two degenerate orbitals that transform as the *E* irreducible representation (e-orbitals) and two separate orbitals of A_1 symmetry (a_1-orbitals). One a_1-orbital is always occupied by two electrons, leaving three possible electronic configurations: $a_1^2e^2$, a_1e^3 and e^4. Taking into account the electron–electron Coulomb interaction leads to the separation of the multi-electron states into triplet (spin S=1) ^{3}A$_2$ and ^{3}E, and singlet (spin S=1/2) ^{1}E and ^{1}A$_1$ levels (**Figure 2a**). It was deduced from hole burning spectra and temperature dependence of magnetic circular dichroism signal[11] that the ground state is the triplet ^{3}A$_2$, and that the PL originate from the excited triplet state ^{3}E→^{3}A$_2$ transition. The ^{3}E excited state is an orbital doublet. Its degeneracy is lifted by nonaxial strain into two orbital branches E_x and E_y, each of them being formed by three spin states S_x, S_y, and S_z, resulting in six different levels that can be observed at cryogenic temperature[12]. For the ground ^{3}A$_2$ triplet level, the spin-spin interaction is responsible for a zero field splitting, *i.e.* a separation between m_S=0 and m_S=±1 of D=2.88 GHz (*i.e.* in the microwave domain). The energy order of the spin projections (along N-V crystallographic direction) m_S = 0, ±1 of the ^{3}A$_2$ triplet, leading to m_S = 0 as the lowest energy state, was assessed by Raman heterodyne-detected-electron-nuclear double resonance[13].

Importantly, at room temperature the ^{3}E excited state fine structure is impacted by phonon mediated averaging of the two low-temperature fine structure branches[14], resulting in only three detectable levels of spin projection m_S=0 and m_S=±1 separated by a zero field splitting D'=1.42 GHz due to the spin-orbit coupling in this case (**Figure 4**).

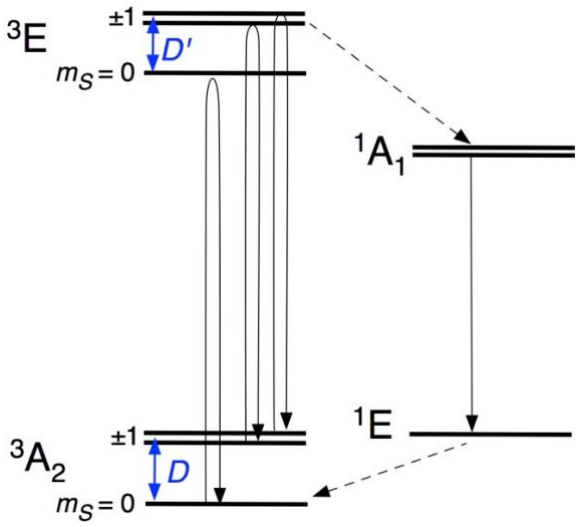

Figure 4 – Fine structure of electronic levels of NV^- center at room temperature, without strain. This structure is the result of phonon mediated averaging of the two low-temperature fine structure branches (total of 6 levels).[14] D=2.88 GHz and D'=1.42 GHz are the zero-field splitting of the ground and excited states respectively. Plain arrows display spin projection m_S preserving transition, while dashed arrows indicates intersystem crossing (non radiative). The polarization of NV^- in m_S=0 ground state spin projection by optical pumping is made possible by these intersystem crossing that takes place mainly from m_S=±1 excited state.

The relative energy positions of the intermediate ^1E and ^1A singlet states has long been debated. A near-infrared (NIR) emission with a ZPL at 1042 nm has been recently reported[15] and based on uniaxial stress measurements it was attributed to the $^1E \leftrightarrow {}^1A$ transition (or $^1E' \leftrightarrow {}^1A$ in Ref.[16]). The NIR emission intensity is about four orders of magnitude weaker, and has a lifetime of about 1 ns[17], both observations indicating a decay dominated by non-radiative pathways. Very recently, further uniaxial stress measurements (shifts and splitting) at cryogenic temperature interpreted with the electronic model of NV^- center, provided evidence for ^1E to be the lower energy state of the intermediate states system (as displayed on **Figure 4**), and also indicated that the large splitting of the 1042 nm ZPL observed under stress is most likely due to electron-electron interaction[18].

The neutral NV^0 has attracted less attention than NV^- because it was hard to detect its EPR signature. NV^0 has five electrons associated to an always occupied a_1-orbitals and, in the ground state, to the a_1^2e configuration yielding the multiple electron ground state ^2E. When an electron is promoted from the singlet to the excited doublet, the configuration becomes $(a'_1{}^2)a_1{}^1e^2$ with associated multiple electron states $^2A_1$, $^4A_2$ and ^2E (**Figure 3a**). The observation by EPR of spin S=3/2 $^4A_2$ level populated by optical excitation was realized only recently[19], and the S=1/2 has ^2E still never been detected by the same approach, probably due to molecular orbitals distortions.

Optically Detected Magnetic Resonance and spin polarization

The strong interest of a broad community (point defect in solid, nanomagnetism, quantum information processing, quantum optics…) for the negatively charged NV^- center stems from its optically detectable spin S=1 ground states. Optical Detection of Magnetic Resonance (ODMR) is a double resonance technique combining optical detection with electron spin resonance spectroscopy. It was initially realized using the phosphorescence (triplet state transitions) of aromatic molecules embedded in crystals, first in ensemble [20,21] and later, owing to the improvement of optical detection techniques, at the level of single molecule[22]. ODMR signal is present only under the right experimental conditions (i.e. with appropriate transition rates) for which the magnetic resonance transitions between the spin sublevels of a triplet state produce changes in the system luminescence. The NV^-

center meets these conditions, and like for molecules, ODMR was first observed in ensemble[23], and then at the single emitter level[24], paving the way to the huge variety of the afore mentioned applications.

The polarization selection rules inferred from group theory[25] indicate that $^3A_2 \leftrightarrow {}^3E$ transitions are orbitally allowed. Moreover, the electrical dipolar operator cannot change the spin projection m_S. Therefore $^3A_2 \leftrightarrow {}^3E$ transitions can only happened with $\Delta m_S=0$ (see curved arrows on **Figure 4**). The NV center is usually excited off-resonance with a laser of higher energy than the one of the ZPL transition, leading to the population of the excited state vibronic levels first and then, by non-radiative decay, towards one of the three possible ^3E sublevels $m_S=0$ or $m_S=\pm1$. Intravibronic transition does not affect the spin projection, so that m_S is preserved throughout the excitation-emission cycle, between either $m_S=0$, $m_S=+1$ or $m_S=-1$. If the system were closed, the transition intensities would be similar. However, the addition of a microwave (MW) field with a frequency tuned at the zero field splitting value of 2.88 GHz leads to a decrease of NV^- luminescence (**Figure 4**). The MW field induces a transfer of population from $m_S=0$ to $m_S=\pm1$. The photoluminescence intensity decrease at the MW resonant frequency (signature of ODMR) indicates that the transitions in the $m_S=+1$ or $m_S=-1$ subsystems are dimmer than the one in the $m_S=0$ subsystem, which is why the ground $m_S=0$ substate is often called the "bright" state.

The origin of NV^- center ODMR stems from the intersystem (triplet⟶singlet) crossing $^3E \longrightarrow {}^1A$ made possible by spin-orbit coupling which mixes triplet and singlet[26]. This mixing allows relaxation between states that transforms with the same symmetry, and calculations indicates that the transfer is predominantly from $m_S=\pm1$. Therefore ^3E, $m_S=\pm1$ levels have an additional decay pathway through the single levels, which explains why $^3E(m_S=\pm1) \longrightarrow {}^3A_2(m_S=\pm1)$ transitions are associated to a dimmer emission compared to $^3E(m_S=0) \longrightarrow {}^3A_2(m_S=0)$ one.

Moreover, it has been known for a long time that strong EPR signal from NV^- center ground state comes from its polarization by light excitation (optical pumping)[5] with a preferred orientation in the $^3A_2$, $m_S=0$ sublevel[27]. This property is also at the heart of quantum measurements based on NV^- center. Like in the case of ODRM, the interpretation of this spin polarization by light involves intersystem crossing $^3E \longrightarrow {}^1A$, but a full understanding of the spin polarization mechanism is still lacking. Indeed, after $^3E \longrightarrow {}^1A$ intersystem crossing ^1A decays to ^1E by emitting light at 1042 nm wavelength. Then ^1E decays non radiatively towards $^3A_2$. Symmetry rules indicate a decay preferentially into E symmetry states (*i.e.* states with $m_S=\pm1$ spin projection) [9,28], but this is in contradiction with the observed polarization in $m_S=0$ state[27]. The spin polarization (change of $m_S=\pm1$ to $m_S=0$) therefore results from a forbidden singlet-triplet transitions that can be explained by first order terms of spin-orbit interaction (indirectly accessible experimentally)[9].

NV center production in nanodiamond: state of the art and challenges

The production of NV centers in nanodiamonds involves a similar treatment as the one in bulk diamond slab, *i.e.* the creation of vacancies by high energy particle irradiation in synthetic diamond followed by high temperature (800-900°C) annealing[29] required for the vacancies to migrate and eventually stabilize in lattice sites adjacent to nitrogen atoms. The vast majority of synthetic diamond used is produced by HPHT method naturally containing nitrogen impurities in substitution of carbon atoms. However, nanodiamonds synthesized by detonation process (leading to particle primary size ≈5 nm) have also been used but NV center photoluminescence is less stable in these ultra small nanocrystallites[29], because the centers are within distance to the surface allowing energy transfer to defects that offer many non-radiative decay pathways. The high energy (a few keV to a few MeV) particles employed for irradiation are either electrons, protons, or helium He^+ ions (and occasionally neutrons[7]). The particles displace the carbon atoms at interstitial positions, leaving a vacancy behind.

To selectively produce NV^- center and not the neutral form NV^0 it has been demonstrated that a concentration of a few 100 ppm is required[30] (type 1b HPHT diamond), and that based on the following two-steps conversion mechanism $V^0 + 2N^0 \rightarrow NV^0 + N^0 \rightarrow NV^- + N^+$, the negative charge is gained from one nitrogen atom a few lattices apart from the NV center considered. Therefore, considering a 100 ppm nitrogen impurity concentration, the maximum reachable NV^- concentration should be 50 ppm[31], *i.e.* 50% conversion rate. Moreover, starting from 10 ppm nitrogen concentration would not allow the production of NV^-.

For application to biolabeling, the largest concentration in NV centers is sought to obtained the brightest possible nanoparticles. A mass production method is also necessary. To this aim two approaches are used (**Figure 5**): (i) direct irradiation and annealing of commercially available nanocrystals, or (ii) irradiation and annealing of HPHT microcrystals (size ≈150-190 µm) followed by their milling into nanocrystals. After either one of these treatments, some graphitic layers and sp^2 carbon phases appear at the surface that need to be removed because they provide additional non-radiative decay pathways and contains also traps of the electronic charge[32] of NV^-.

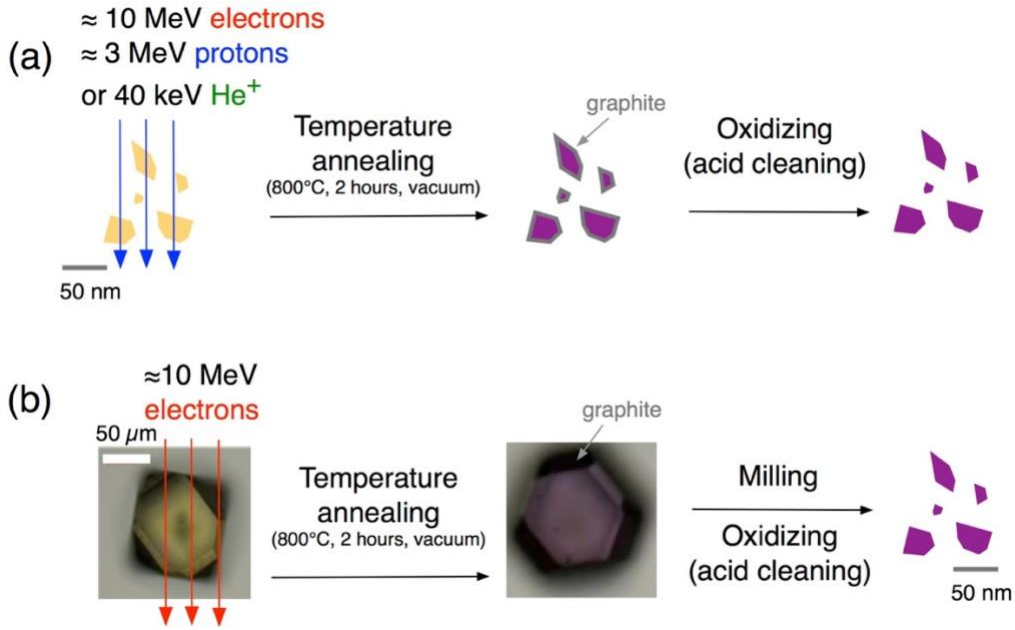

Figure 5 – Process of fluorescent nanodiamond synthesis. (a) Direct irradiation of synthetic nanodiamond (obtained by milling faceted HPHT microdiamonds, containing ≈100 ppm nitrogen impurities) with high energy particles (protons, electron or helium ions, depending on the amount of material to treat) followed by 800°C vacuum annealing, and oxidizing (450°C in air, or/and strong acid cleaning) to remove amorphous sp^2 graphitic layer formed during irradiation and the annealing. (b) Irradiation of the HPHT size≈150 µm microcrystals, followed by high temperature annealing, milling down to size<50 nm nanoparticles and oxidation to remove amorphous carbon.

The first mass production technique based on irradiation of nanocrystals was developed by Chang et al.[29] using a 40 keV energy He^+ ion beam for irradiation (**Figure 5a**). In this technique nanodiamonds of size<50 nm are deposited in a monolayer (because of small penetration depth of 40 keV He^+) on a few meters long copper ribbon that is slowly moved in front of the ion beam. The advantage of such an approach is the use of a compact ion source that can be installed in any laboratory, while proton or electron accelerators are larger equipments subject to constraining safety regulations. Moreover, one 40 keV He^+ produce ≈40 vacancies when it penetrates into diamond, while 2 MeV electron and 3 MeV proton beams create 0.1 and 13 vacancies respectively[29]. However, larger fluences can be achieved with these two types of beams, compensating for this difference in damage production: up to 10^{20} electrons/cm^2 with 10 MeV electrons[33] and 10^{17} protons/cm^2 with 2.4 MeV protons[34], compared to $6x10^{13}$ He^+/cm^2. In addition, the large penetration depth of high energy electrons (1-2 cm for 10 MeV electron, the exact value depending on the design of the reactor in which the diamond powder is placed) allows to treat a large amount (up to a few grams) at once[35–37].

The second mass production approach consisting in irradiating microcrystals before their milling into nanoparticles (**Figure 5b**), was expected to yield higher concentration of NV centers. N-V complex formation requires the migration of the vacancies during the annealing process, and applying this treatment to microcrystals

instead of nanocrystals should reduce the annihilation of the vacancy at the surface[35]. However, this top-down production approach did not yield higher NV^- concentration compared to direct irradiation of ND, as revealed by photoluminescence and EPR measurement[38]. The smallest reported fluorescent ND (FND) containing at least one NV^- center (charge state assessed by PL and ODMR measurements) have a size in the 5-10 nm range[33,39].

Currently the highest concentrated FNDs of size ≈30 nm contain in average about 15 NV centers, corresponding to about 19 ppm, which would be associated to about 10% conversion efficiency of nitrogen into NV centers in a 200 ppm nitrogen concentrated sample. These bright FNDs are produced by 3 MeV proton beam irradiation[31] at fluence of $2x10^{16}$ protons/cm^2. Like in the case of bulk diamond[34], further increase of the fluence did not result in an increase of NV concentration. Moreover, the use of starting materials containing increasing nitrogen impurities from 100 to 200 ppm resulted in a concomitant increase of NV concentration as expected, but ND with larger N^0 concentration of ≈400 ppm yielded a NV concentration similar to the one with 100 ppm N^0. This disappointing observation may be due to the presence of structural defects in this highly N-doped diamond, that impact NV center formation[31].

The main application of FND are in the fields of bioimaging, physico-chemical sensing[40,41] and scanning probe magnetometry[42]. In most of these fields, decreasing the FND size while increasing the NV concentration would enhance the possibilities of applications. In particular, for biolabelling FND of size <10 nm would give access to region of interest hardly accessible due to steric hindrance, like the synaptic cleft or the dendritic spine neck of neurons. Current challenges in the field of NV center production in nanodiamonds are thus the following: (i) increase the production yield of size<10 nm FND; (ii) increase FND brightness, by increasing the nitrogen→ NV conversion efficiency; (iii) improve FND size and brightness homogeneity. Regarding the later point, irradiation of ND in liquid phase showed a reduced dispersion of FND brightness[43], attributed to more homogeneous irradiation dose per particle as a consequence of thermal agitation.

Different excitation modalities and photophysical parameters

Thanks to their remarkable photostability, NV center in nanodiamond can be excited and then observed on a very long time scale, using either a laser beam (PL) as previously discussed or with an electron beam (Cathodoluminescence[44,45], CL) in a scanning electron microscope (EM). In the later case it is possible to get simultaneously an EM contrast (for example the bright field or high angle angular dark field[45]) with nanometer resolution and a CL image perfectly correlated (**Figure 6**). Such integrated correlative microscopy may become an invaluable method for cellular imaging[46], allowing to observe simultaneously the cell ultrastructure and the FND label, provided the FND has been functionalized to recognize the target of interest.

Regarding the radiative lifetime, different measurements gave values different for m_S=0 → m_S=0 or m_S=±1 → m_S=±1 transitions (see Table 10 of Ref. [8]): 11.6 to 13.7 ns for NV^- in bulk diamond at room temperature for the transition ^3E m_S=0 → $^3A_2$ m_S=0, and 7.3-7.8 ns ^3E m_S=±1 → $^3A_2$ m_S=±1. However, the diamond nanoparticle host being smaller than NV emission wavelength, it modifies the local density of states of the electromagnetic modes and therefore the radiative lifetime which can be strongly increased in such an electrostatic limit[47,48]. Indeed, in practice, due to the presence of numerous non radiative channels[49], radiative lifetime of NV^- in nanodiamond is broadly distributed in the 10-40 ns range, with the most frequent value being 33 ns for 100 nm sized nanoparticle and 28 nm for 25 nm sized ones. Despite a smaller radiative lifetime increase than the one that can be expected from electromagnetism theory, values around 30 ns are about one order of magnitude larger than radiative lifetime of autofluorescence which is in the 1-4 ns range (depending on the endogenous pigment). Therefore, using Fluorescence Lifetime Imaging Microscopy (FLIM) or simply by time delayed detection (in time window starting from ≈10 ns), one can filter out photons from NV^- emission on a nearly dark background and strongly improve the signal to background ratio of fluorescent nanodiamond imaging[50]. Such FLIM or time-delayed detection has been used to investigate the tissue distribution of nanodiamonds after injection in *Caenorhabditis elegans* worm[51] (**Figure 7**) or in mouse lung sections[52].

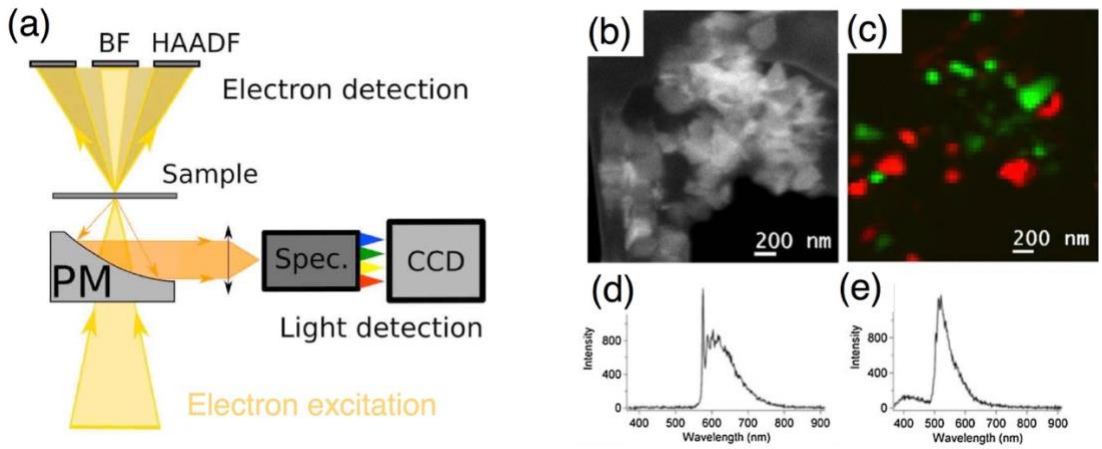

Figure 6 – Integrated spectrally resolved cathodoluminescence (CL) and scanning electron microscopy (STEM). (a) CL-STEM setup. The electron beam (energy ≈80 keV) comes from the bottom, crosses a parabolic optical mirror (PM), then hit the sample and yields a bright field (BF) or high angled annular dark field (HAADF) TEM image on the electron detectors. The PM directs the CL light towards an imaging spectrograph made of a monochromator (Spec.) and a CCD array detector. (b) HAADF image of a mixture of natural and HPHT nanodiamonds displaying either a green emission (from N-V-N defect centers, also known as H_3) or red emission (from NV^0) centers, with the corresponding spectra ((d) for NV^0 and (e) for H_3). The sample holder temperature is about 100 K, which explains that the ZPL of NV^0 is narrower than on Figure 3b room temperature PL spectra. (b)-(e) are adapted from Ref.[77] with permission, ©2013 Wiley.

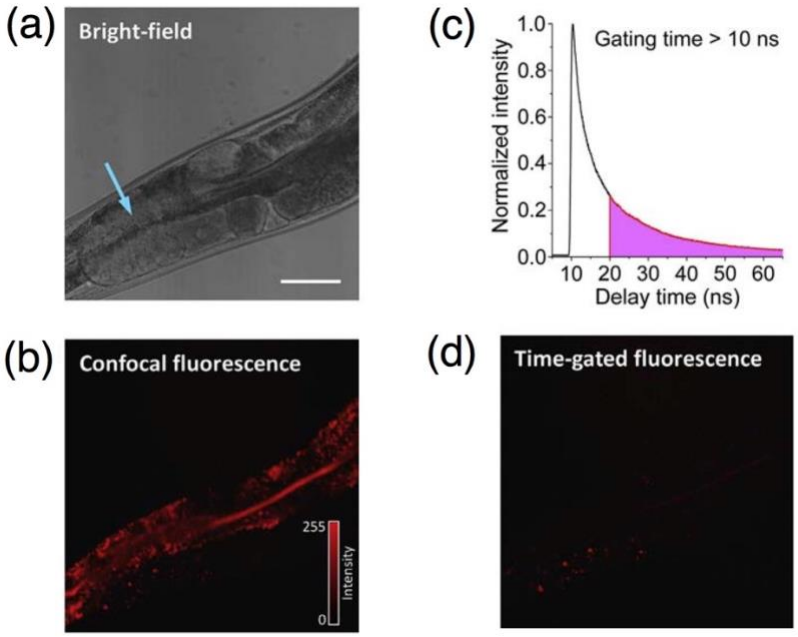

Figure 7 – Background-free imaging of fluorescent nanodiamond in living *C. elegans* worm, based on time delayed detection. (a) White light (bright-field) imaging of a portion of a living *C.* elegans worm. The blue arrow indicates the location of FNDs injection. Scale bar: 50 µm. (b) Fluorescence confocal raster scan of the same region than in (a), showing the FNDs and the worm autofluoresence. (c) Fluorescence decay time trace of size≈100 nm FNDs suspended in water. The area shaded in magenta represents the fluorescence signal collected at the gating times longer than 10 ns. (d) Time-delayed fluorescence raster scan displaying only FNDs fluorescence on a dark autofluorescence background, which allows non ambiguous identification of FNDs within the work body. Adapted from Ref.[51] with permission, © Elsevier 2013.

Finally, since bright FNDs are intended to be used as fluorescent bioimaging labels, it is of interest to compare their brightness to the one of standard fluorescent nanoparticles like semiconductors nanocrystals (quantum dots, QDs). Such comparison was done in scanning confocal microscopy on single emitters of each type (single NV center in a nanodiamond, and single QD)[53]. It revealed that the excitation saturation intensity is 75 times larger for one NV center in a ND, compared to a single QD, and that the maximum detection rate was about 3 times larger for the QD than for the NV center. These data indicate that a FND containing more than 3 NV centers will be brighter than a single QD, but one also needs to use a higher excitation power. This later requirement is the consequence of two phenomena: (i) a larger scattering of incident light by the diamond crystal than by the QD, and (ii) about one order of magnitude smaller absorption cross-section of NV center compared to QD.

High-resolution optical microscopy with FND in photo- and cathodoluminescence (see Chap. 19 too)

Owing to its very high stability under photon or electron beam irradiation, fluorescent nanodiamonds have been used in super-resolution microscopy. The record resolution ever achieved with STimulated Emission Depletion microscopy (which is only limited by the stimulated laser beam power that can be sustained by the sample) was obtained for single NV center in bulk diamond, down to 2.4 nm[54]. In 80 nm sized nanodiamond, STED also allowed to image individual NV centers with a resolution of ≈10 nm[55], that was limited by thermal drift due to residual absorption of the STED laser beam which maximum mean power was about 1 W, focused onto the FND.

By integrating a pierced parabolic mirror into a Scanning Transmission Electron Microscopy (STEM), with its focal point located at the sample position, Kociak *et al.* obtained a cathodoluminescence image of a single NV center in a nanodiamond with a sub-wavelength optical resolution of about 100 nm[56]. In such experiment, the NV center is promoted in its excited state by the recombination of excitons travelling inside the diamond lattice. These excitons result from the de-excitation of a plasmon generated by the interaction of the fast electrons with the diamond material. The optical resolution limit in CL may correspond to the exciton mean free path before their recombination and subsequent NV center excitation.

7.2 The Silicon-Vacancy centers in nanodiamonds

Silicon-vacancy (SiV) color centers possess a number of advantages in its optical properties over NV centers in nanodiamond. Zero-phonon emission from Si-V defects is observed at wavelength of 738 nm which is away from the characteristic broad-band (450-650 nm) photoluminescence of ND. Narrowband (a few nanometers) zero-phonon emission is a few percent for the NV centers, whereas it is 70–80% for SiV centers. Both centers demonstrate photo stability and high quantum yield of luminescence even at room temperature. Listed properties of the SiV centers make NDs, containing these centers, promising for application as photoluminescent biomarkers and as single-photon emitters.

Photoluminescent spectrum and electronic structure of the silicon-vacancy color center.

Characteristic photoluminescence spectrum of diamond containing silicon-vacancy centers is shown in **Figure 8.** Luminescence of SiV is mostly localized in a zero-phonon line (ZPL) of the center at 738.5 nm and a weak phonon side-band is placed in the range of 740-820 nm. The ZPL contains 70-80% of the SiV emission, and this feature is favorable for single photon source applications.[57] SiV ZPL splits into four lines at liquid helium temperature.[58] The origin of the splitting is attributed to split ground and excited states (**Figure 9**).

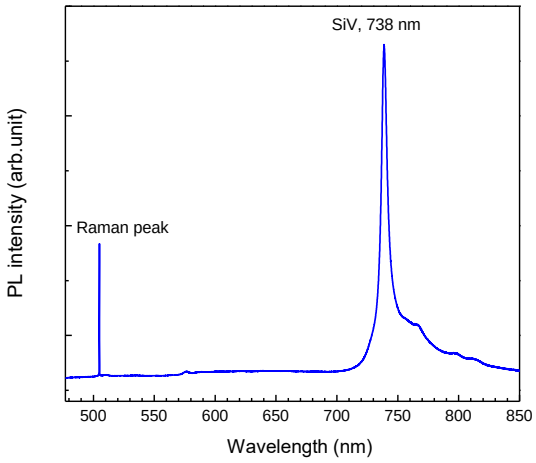

Figure 8 – Characteristic photoluminescence spectrum of diamond containing silicon-vacancy centers emitting at 738 nm.

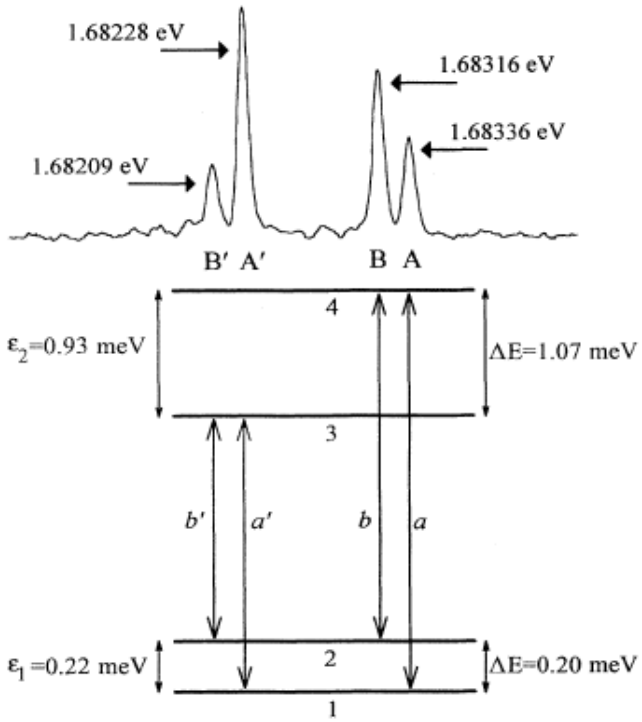

Figure 9 – Absorption spectrum of diamond with SiV centers measured at 6K (top). Proposed energy-level diagram of SiV center (bottom).[58]

The molecular structure of the SiV center was calculated using spin-polarized local density functional cluster theory. Silicon was predicted to be unstable when placed in a lattice site next to a vacancy, spontaneously relaxing into a split-vacancy position. Si atom is located at the centre of a nearest-neighbour divacancy (**Figure 10**) forming the color center of D_{3d} symmetry.[59] Recently the D_{3d} symmetry of the SiV centers was confirmed experimentally.[60,61] The results on comparative study of Si-related centers by electron paramagnetic resonance and photoluminescence spectroscopy suggest a negative charge state for the SiV center emitting at 738 nm.[62] In this connection it is currently designed as SiV^-.

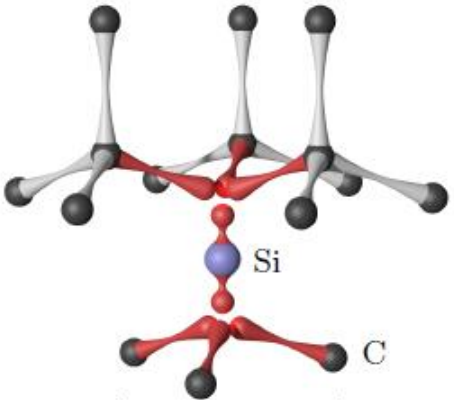

Figure 10 – The molecular structure of the SiV center.

Production of nanodiamonds with SiV^- centers

Nanotechnology applications of SiV^--based luminescent nanodiamonds, in particular their use as luminescent biomarker, is constrained by lack of methods for mass production of such nanomaterial. Below, we discuss the possibility of the main methods of diamond synthesis and the recent results of their use in production of the luminescent NDs.

CVD technique – Chemical vapor deposition (CVD) is a modern technique used for production of polycrystalline and single crystal diamond at typical pressures of ~100 Torr (~0.13 bar)and temperatures in the range 700-1000 °C.[63] In all versions of the CVD synthesis the gas phase comprises a volatile carbonaceous material (methane, alcohols, acetone) and hydrogen. The deposition is carried out from activated gas phase. The main methods of activation - thermal (hot filament) and electric - different forms of discharge (arc, glow) with the use of both DC and AC (microwave pulse mode). Activation of the gas phase creates a sufficiently high concentration of active carbonaceous particles, atomic carbon and hydrogen. The active carbon is the key to the subsequent gas-phase and surface chemical reactions necessary to sustain the growth of the diamond. Created atomic hydrogen etches various forms of non-diamond carbon appearing in the synthesis zone carbide forming metals (W. Mo, Ta, etc.), silicon, or diamond used as substrates for CVD diamond growth. For deposition on non-diamond substrate micro- and nanocrystals of diamond are used as seeds. They are applied to a substrate surface, for example, by sonication.

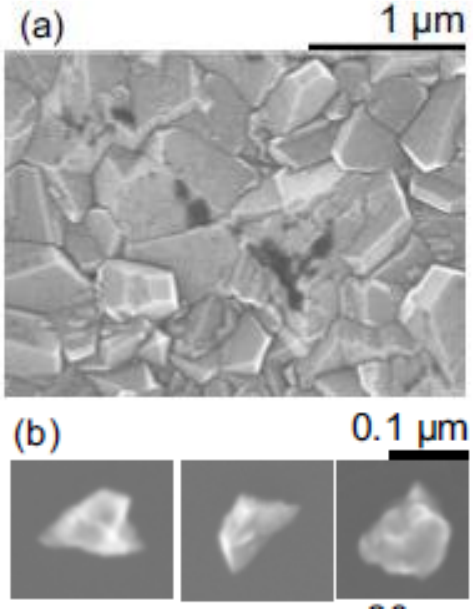

Figure 11 – SEM images of: (a) the polycrystalline starting material, (b) individual NDs after spin coating onto a Si substrate.[65]

The CVD production of isolated diamonds nanoparticles doped with Si is described by H. Zhang et al.[64] SiV^- luminescent nanodiamonds were synthesized by standard CVD technique on silicon substrate, followed by sonication to generate free particles. Typical nanodiamond sizes were found to be in the range of 50–250 nm. Such approach for production of luminescent nanodiamond is extremely ineffective. In one working cycle of CVD diamond deposition (typical time is about 1 hour) only ~0.01 mg of 100 nm diamond particles can be produced. One more way for using of CVD for luminescent ND synthesis was suggested by E. Neu et al..[65] There the production of fluorescent NDs containing *in situ* produced SiV^- centers from polycrystalline CVD films via the bead assisted sonic disintegration (BASD) method is reported. Produced NDs combine the advantageous SiV^- fluorescence properties and its feasible production during the CVD process with the extended applicability of NDs dispersed in solution. Starting material for ND production was a polycrystalline diamond film grown by hot filament CVD on ND seeded Si substrate. Scanning electron microscope (SEM) images indicate a film thickness of 2 µm and high crystalline quality (grain size 0.5–1 µm **Figure 11a**). The characterized diamond film is used for ND production after removing the substrate by chemical etching. The BASD process, disclosed recently,[66] enables the deagglomeration of strongly agglomerated nanoparticles by charging ceramic microbeads to a sonicated suspension. The microjets or shock waves induced by ultrasonic cavitations propel the beads (ZrO_2, 50 µm sized) leading to the disintegration of large agglomerates and the eventual formation of colloidal solutions of primary nanoparticles. So far, the method has only been applied for the deagglomeration of nanoparticles bound by interparticle forces. There, the BASD technique was applied as a top down approach for the production of nanoparticles from a CVD diamond film by separating the grains and crushing the micrometer-sized crystals. The BASD process is followed by several purification steps, delivering a colloidal suspension of NDs in de-ionized water. The average particle size, determined by dynamic light scattering directly in the resulting solution, shows a distribution maximum at 70–80 nm. SEM observation verified the nanometric size of the nanoparticles (**Figure 11b**). The faceted shape of the individual NDs indicates the crushing of the film's crystallites along lattice planes. No contamination from the BASD process was found in the final colloidal solution. **Figure 12** displays a typical fluorescence spectrum of a ND ensemble. Significant reduction in broadband fluorescence was achieved, while the SiV^- luminescence remained basically unchanged (ZPL 738.6 nm, width 6.8 nm). The method of ND production by milling looks more time- and labor-intensive than the direct CVD synthesis of the luminescent NDs. It seems that the size of produced diamond nanoparticles is also limited to 70-80 nm in the milling approach.

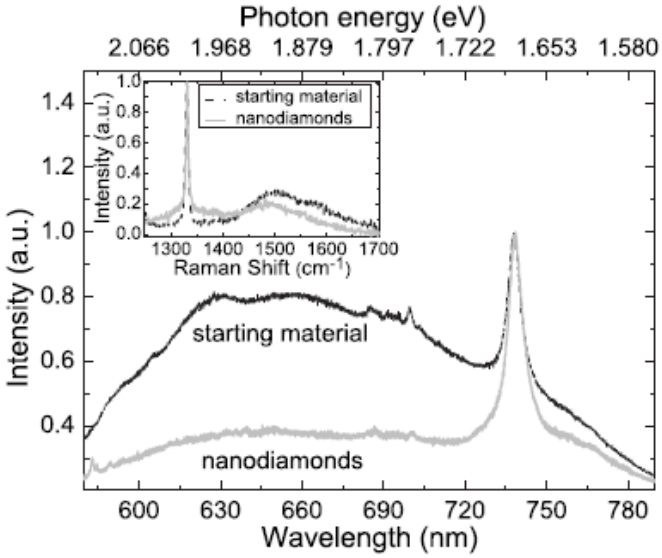

Figure 12 – Photoluminescence spectra recorded under 532 nm laser excitation from the polycrystalline starting material and an ensemble of the produced NDs. The inset shows the Raman spectrum of the starting material and the NDs recorded with 488 nm laser light.

HPHT technique– Currently, there are large-scale industrial production of synthetic diamonds under high temperature and high pressure (HPHT technique). HPHT synthesis occurs usually in the metal (solvent) - carbon (graphite) system. High-pressure (10-20 GPa) are created in the hard-alloy chambers by powerful presses. Diamonds are crystallized during cooling from the melt (a supersaturated solution of carbon in the metal) under pressure. Synthesized diamonds are separated from the sinter by dissolving the matrix in a mixture of acids. Diamond powders for industrial purposes, as well as single crystals of gem quality are produced by HPHT technique. Without a metal solvent, the rate of conversion of graphite into diamond is significantly reduced.
Until recently, HPHT technique has not been used for synthesis of luminescent NDs. In 2014, the preparation of heterogeneous size diamond particles (including nanoscaled) doped with silicon and nitrogen during their synthesis from mixtures of hydrocarbon and fluorocarbon compounds was reported.[67] NV and SiV^- luminescence was observed from nano- and micro-sized fractions of produced diamonds (**Figure 13)**. This result demonstrates a high potential of HPHT technique for a large-scale production of the SiV^--based luminescent nanodiamonds.

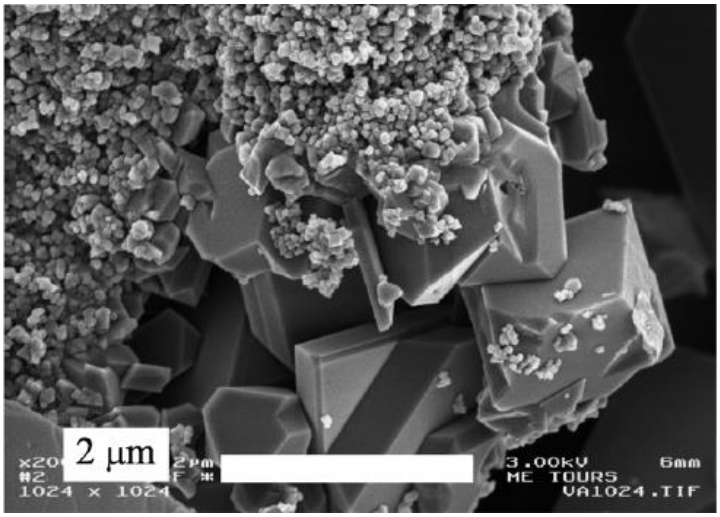

Figure 13 – Scanning electron microscopy images of diamond materials obtained from binary mixture $C_{10}H_8$–$CF_{1.1}$.

Detonation technique – Synthesis of nanodiamonds by detonation loading of explosives with negative oxygen balance is the cheapest and most efficient way to direct production of nanodiamonds with a size of less than 10 nm. Systematical study of main representative classes of NDs produced by detonation shock wave conversion of different carbon precursor materials, namely, graphite, graphite/explosive mixture, and different combinations of pure explosives using different cooling methods (wet or dry cooling) has been carried out by Shenderova et al..[68] SiV^- luminescence was not observed in any of the test detonation nanodiamonds (Si was expected as background impurity in those materials). A large number of samples of detonation nanodiamonds (DND) were produced in a presence of various dopants, including silicon.[69] PL study of these samples in our lab did not reveal any SiV^- luminescence in them. Thus, for today, the detonation technique remain unpromising for production of the SiV^--based luminescent nanodiamonds.

Size depended luminescence of SiV^- centers.

In developing SiV^--based luminescent nanodiamonds two main questions have to be answered: (1) how thermodynamic stability of the SiV^- formation depends on a size of diamond nanoparticle, and (2) at which distance of SiV^- defect from the surface of nanodiamond a defect-surface interaction becomes essential.

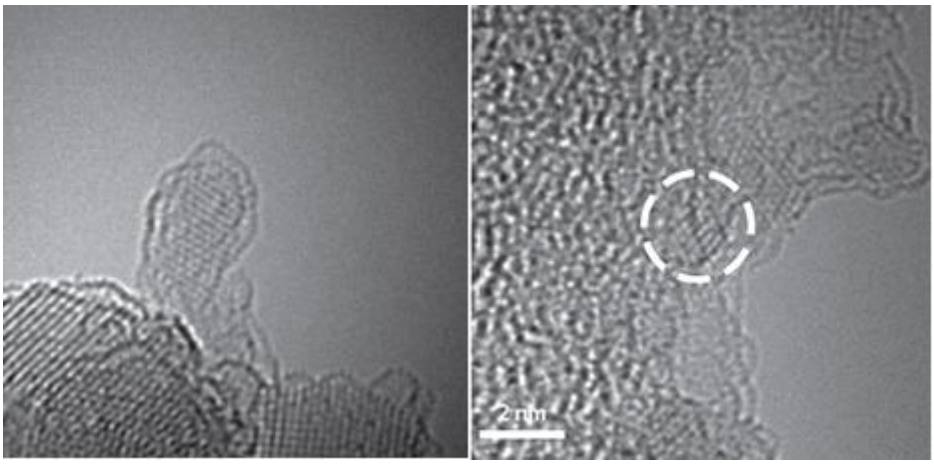

Figure 14 – High-resolution TEM images of meteorite nanodiamonds: (a) free standing grain (2-nm size), (b) grain (1-nm size) in agglomerate.[73]

Calculations have predicted nitrogen to be thermodynamically unstable in nanodiamonds with less than 2 nm in sizes.[70] In contrast, silicon-vacancy defects in hydrogen-passivated truncated octahedral nanodiamonds have been predicted theoretically to be stable in particles of ≈2 nm in diameter.[71,72] Later simulations indicated that the SiV^- centres are thermodynamically stable even in nanodiamonds with sizes ranging from 1.1 nm to 1.8 nm.[73] Smallest ND shown SiV^- luminescence was found under study of ND extracted from stony meteorite.[73] Some fraction of meteorite ND has a size below 2 nm (**Figure 14**). Namely individual particles of this fraction predominantly contained one or even a few SiV^- centers. Number of the centers in diamond nanoparticle is determined by measuring the time autocorrelation function $g^{(2)}$ of the SiV^- luminescence intensity for individual particle (**Figure 15**). The SiV^- emission shown blinking but was stable (no bleaching) over a few hours. Blinking of the SiV^- emission we relate to the interaction of the centers with closely located defects of diamond surface.

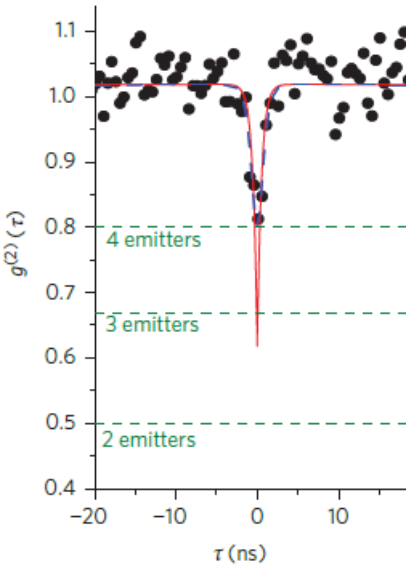

Figure 15 – An autocorrelation function showing the background corrected raw data fitted with a model including the instrument response. The number of emitters within the analyzed spot was found to be 3.

In common case a decreasing size of ND containing color centers increases possibility of their interaction with the diamond surface that usually suppresses the ND luminescence. This happens at changing charge state of the centers by surface acceptors or/and the emission interruption (the luminescence blinking) until electrons are released back from the surface defects trapping the electrons.[74] A minimum distance of SiV^- and NV^- centers from

nanodiamond surface at which these centers cease to "feel" the diamond surface was evaluated by V.A. Shershulin et al.[75] The studied diamond nanoparticles presented a composite structure of "core-outer layer" type. The core was 20-nm HPHT diamond particle containing NV^- centers, whereas outer diamond layer containing SiV^- centers was formed by CVD synthesis (**Figure 16**). The blinking of NV^- emission was found for all samples besides the sample with 44 nm particles (12 nm CVD layer). Duration of the "off" states of NV^- centers was reduced with CVD layer thickness, and the blinking completely disappeared for 44-nm diamond particles. Thus, the 12 nm thickness of CVD layer can be considered as a minimum distance between NV^- centers and ND surface at which their interaction is no longer takes place. The 738 nm emission (ZPL) of SiV^- centers was not revealed until the particle size reaches 28 nm (4 nm CVD layer). The dramatic increment in SiV^- emission happened when the CVD layer increased by 4 nm, from 8 nm to 12 nm (**Figure 17**). This effect was interpreted as termination of SiV^- luminescence suppression by surface defects. Thus, the value of 4 nm may be considered as a critical distance from SiV^- to the diamond surface larger of which the interaction between SiV^- and diamond surface becomes insignificant. This finding determines a minimum size of nanodiamonds, in which stable luminescent centers could be effectively formed, namely, 8 nm for SiV^- emitters and 24 nm for NV^- emitters.

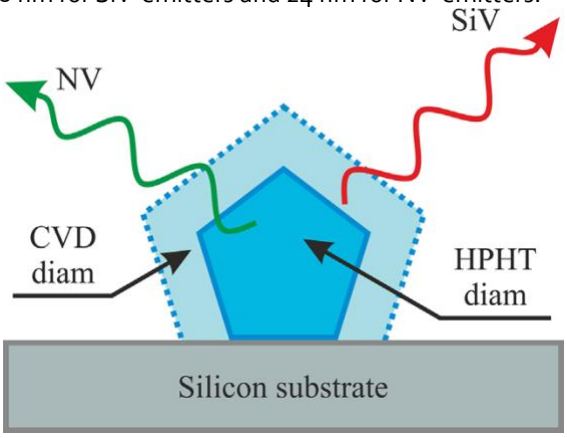

Figure 16 –. Schematic representation of the studied diamond nanoparticles presenting composite structure of "core-outer layer" type. The core is 20 nm HPHT diamond containing NV centers, whereas outer diamond layer containing SiV^- centers is formed by CVD synthesis.

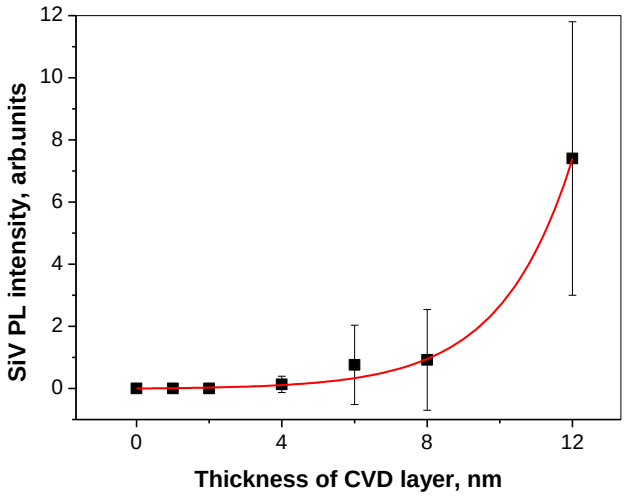

Figure 17 –. Dependence of SiV^- luminescence intensity on the thickness of CVD diamond layer.

Application of SiV^- -containing NDs as luminescent biomarkers.

The use of NDs hosting SiV^- defects as effective biomarkers of primary neural precursor cells (NPCs) isolated from the adult mouse brain has been reported by T.D. Merson et al.[76] SiV^- centers were produced in 40 nm high-

pressure high-temperature NDs by implantation of Si with dose of 10^{17} Si ions/cm^2 into the ND powder at room temperature. After implantation, NDs were annealed for 1 h in forming gas to create the defects and remove residual graphite. To examine the spectral properties of SiV^- -containing NDs for cellular labeling, NPCs were cultured for 4 days as suspension cultures with 40 nm NDs implanted with Si. It was found that NDs containing SiV^- defects labeled cells with great efficiency. **Figure 18** shows a confocal image collected using an Olympus FV-1000 microscope of NPCs cultured with 40 nm SiV^- -implanted NDs. The pseudocolored luminescent signal illustrates the range of luminescent intensities detected among labeled cells. Extremely small use of SiV^- -based luminescent nanodiamonds as luminescent biomarker is explained by lack of methods for mass production of such nanomaterial.

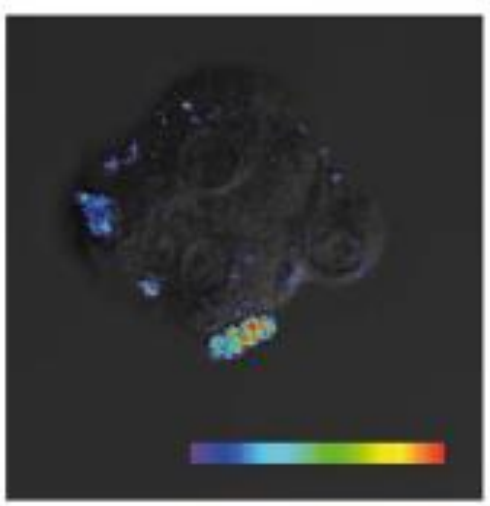

Figure 18. A confocal image of NPCs grown on NDs merged with a bright field image of the neurosphere in grayscale collected by Nomarski optics revealing the exceptional contrast of SiV^- -containing NDs over cell background.

7.3 Conclusion

Nanodiamond can have various embedded light emitters, among which the most prominent ones are the NV and SiV color centers presented in this chapter, and that emit in the far red and near infrared spectral regions. Both emitters-embedded in nanodiamonds can be observed in photoluminescence or cathodoluminescence and have a very stable emission with a high quantum yield. Moreover, each of them have additional remarkable properties.

The negatively charged NV^- center has a spin triplet ground state that can be optically polarized. Moreover, it has an electron spin resonance that can be detected optically so that NV^- in nanodiamond have been used as non invasive (optical) nanoscale magnetic sensors, or sensors of paramagnetic ions with high sensitivity. Finally, NV^- center containing nanodiamond can be produced in mass (grams) which facilitate their application in bioimaging in particular.

However, one drawback of the NV center is its broad emission spectrum of ≈100 nm width, limiting the possibility of multiplexing this fluorophore with only two other colors (green emission like the one of fluorescein and blue emission, like the one of DAPI dye). In comparison, the negatively charged SiV^- center has an emission spectrum mostly contained in the zero-phonon line centered at 738.5 nm and only ≈2-nm broad.

There are various productions methods of SiV-containing nanodiamonds either by CVD process of HPHT approaches but none of them has achieved the same production yield than NV-embedded ND, which is why applications of SiV-ND, in particular in bioimaging, have been very limited until now. This may change in a near future because the production of SiV-doped micro- and nanodiamonds by the industrial large scale HPHT process was recently achieved, starting from a mixture of hydrocarbon and fluorocarbon compounds.

In this chapter, we have shown why NV- or SiV-containing nanodiamonds are unique imaging nanolabels and nanosensors of a broad range of applications. Their production is becoming a mature technology. However, there are still some challenges to address. In particular, the smallest fluorescent ND used in applications up to now have

a size of ≈30 nm, but other demanding applications require much smaller size, eventually limited by non-radiative decay towards surface defects which would correspond to a size of a few nanometers. Moreover, a well controlled and versatile bio-functionalization is still lacking. Therefore, research efforts now focus on (i) increasing the production yield of size<10 nm fluorescent nanodiamonds and (ii) grafting functional bio-molecule (*e.g.* antibody) on the nanoparticle, to eventually reduce the gap (in terms of size) between photostable nanodiamonds and bleaching organic fluorophores.

Acknowledgements
This work was supported by Russian Science Foundation (grant No.14-12-01329), by a public grant overseen by the French National Research Agency (ANR) as part of the "Investissements d'Avenir" program (Labex NanoSaclay, reference: ANR-10-LABX-0035), and by ANR grant No 2010-INTB-1002.

References

(1) Dyer, H. B.; Raal, F. A.; Du Preez, L.; Loubser, J. H. N. Optical Absorption Features Associated with Paramagnetic Nitrogen in Diamond. *Philos. Mag.* **1965**, *11*, 763–774.
(2) Du Preez, L. Electron Paramagnetic Resonance and Optical Investigations of Defect Centres in Diamond., University of the Witwatersrand (South Africa), 1965.
(3) Clark, C. D.; Norris, C. A. Photoluminescence Associated with the 1.673, 1.944 and 2.498 eV Centres in Diamond. *J. Phys. C Solid State Phys.* **1971**, *4*, 2223–2229.
(4) Davies, G.; Hamer, M. F. Optical Studies of the 1.945 eV Vibronic Band in Diamond. *Proc. R. Soc. A Math. Phys. Eng. Sci.* **1976**, *348*, 285–298.
(5) Loubser, J. H. N.; Van Wyk, J. A. Optical Spin-Polarisation in a Triplet State in Irradiated and Annealed Type 1b Diamonds. *Diam. Res.* **1977**, *9*, 11–14.
(6) Loubser, J. H. . J.; van Wyk, J. A.; Wyk, J. van. Electron Spin Resonance in the Study of Diamond. *Reports Prog. Phys.* **1978**, *41*, 1201.
(7) Mita, Y. Change of Absorption Spectra in Type-Ib Diamond with Heavy Neutron Irradiation. *Phys. Rev. B* **1996**, *53*, 11360.
(8) Doherty, M. W.; Manson, N. B.; Delaney, P.; Jelezko, F.; Wrachtrup, J.; Hollenberg, L. C. L. The Nitrogen-Vacancy Colour Centre in Diamond. *Phys. Rep.* **2013**, *528*, 1–45.
(9) Doherty, M. W.; Manson, N. B.; Delaney, P.; Hollenberg, L. C. L. The Negatively Charged Nitrogen-Vacancy Centre in Diamond: The Electronic Solution. *New J. Phys.* **2011**, *13*, 025019.
(10) Coulson, C. A.; Kearsley, M. J. Colour Centres in Irradiated Diamonds. I. *Proc. R. Soc. A Math. Phys. Eng. Sci.* **1957**, *241*, 433–454.
(11) Reddy, N. R. S.; Manson, N. B.; Krausz, E. R. Two-Laser Spectral Hole Burning in a Colour Centre in Diamond. *J. Lumin.* **1987**, *38*, 46–47.
(12) Batalov, a.; Jacques, V.; Kaiser, F.; Siyushev, P.; Neumann, P.; Rogers, L. J.; McMurtrie, R. L.; Manson, N. B.; Jelezko, F.; Wrachtrup, J. Low Temperature Studies of the Excited-State Structure of Negatively Charged Nitrogen-Vacancy Color Centers in Diamond. *Phys. Rev. Lett.* **2009**, *102*, 1–4.
(13) Manson, N. B.; He, X. F.; Fisk, P. T. Raman Heterodyne Detected Electron-Nuclear-Double-Resonance Measurements of the Nitrogen-Vacancy Center in Diamond. *Opt. Lett.* **1990**, *15*, 1094–1096.
(14) Rogers, L. J.; McMurtrie, R. L.; Sellars, M. J.; Manson, N. B. Time-Averaging within the Excited State of the Nitrogen-Vacancy Centre in Diamond. *New J. Phys.* **2009**, *11*, 063007.
(15) Rogers, L. J.; Armstrong, S.; Sellars, M. J.; Manson, N. B. Infrared Emission of the NV Centre in Diamond: Zeeman and Uniaxial Stress Studies. *New J. Phys.* **2008**, *10*, 103024.
(16) Ma, Y.; Rohlfing, M.; Gali, A. Excited States of the Negatively Charged Nitrogen-Vacancy Color Center in Diamond. *Phys. Rev. B - Condens. Matter Mater. Phys.* **2010**, *81*, 1–4.
(17) Acosta, V. M.; Jarmola, A.; Bauch, E.; Budker, D. Optical Properties of the Nitrogen-Vacancy Singlet Levels in Diamond. *Phys. Rev. B* **2010**, *82*, 201202.
(18) Rogers, L. J.; Doherty, M. W.; Barson, M. S. J.; Onoda, S.; Ohshima, T.; Manson, N. B. Singlet Levels of the NV – Centre in Diamond. *New J. Phys.* **2015**, *17*, 013048.
(19) Felton, S.; Edmonds, a.; Newton, M.; Martineau, P.; Fisher, D.; Twitchen, D. Electron paramagnetic resonance studies of the neutral nitrogen vacancy in diamond. *Phys. Rev. B* **2008**, *77*, 1–4.
(20) Kwiram, A. L. Optical Detection of Paramagnetic Resonance in Phosphorescent Triplet States. *Chem.*

Phys. Lett. **1967**, *1*, 272–275.
(21) Schmidt, J.; Hesselmann, I. A. M.; De Groot, M. S.; Van der Waals, J. H. Optical Detection of Electron Resonance Transitions in Phosphorescent Quinoxaline. *Chem. Phys. Lett.* **1967**, *1*, 434–436.
(22) Wrachtrup, J.; von Borczyskowski, C.; Bernard, J.; Orritt, M.; Brown, R. Optical Detection of Magnetic Resonance in a Single Molecule. *Nature* **1993**, *363*, 244–245.
(23) Oort, E. Van; Manson, N. B.; Glasbeek, M. Optically Detected Spin Coherence of the Diamond N-V Centre in Its Triplet Ground State. *J. Phys. C Solid State Phys.* **1988**, *21*, 4385–4391.
(24) Gruber, A.; Dräbenstedt, A.; Tietz, C.; Fleury, L.; Wrachtrup, J.; von Borczyskowski, C.; Borczyskowski, C. von. Scanning Confocal Optical Microscopy and Magnetic Resonance on Single Defect Centers. *Science (80-.).* **1997**, *276*, 2012–2014.
(25) Maze, J. R.; Gali, A.; Togan, E.; Chu, Y.; Trifonov, A.; Kaxiras, E.; Lukin, M. D. Properties of Nitrogen-Vacancy Centers in Diamond: The Group Theoretic Approach. *New J. Phys.* **2011**, *13*, 025025.
(26) Manson, N. B.; Harrison, J.; Sellars, M. Nitrogen-Vacancy Center in Diamond: Model of the Electronic Structure and Associated Dynamics. *Phys. Rev. B* **2006**, *74*, 104303.
(27) Harrison, J.; Sellars, M. .; Manson, N. . Optical spin polarisation of the N-V centre in diamond. *J. Lumin.* **2004**, *107*, 245–248.
(28) Delaney, P.; Greer, J. C.; Larsson, J. A. Spin-Polarization Mechanisms of the Nitrogen-Vacancy Center in Diamond. *Nano Lett.* **2010**, *10*, 610–614.
(29) Chang, Y.-R.; Lee, H.-Y.; Chen, K.; Chang, C.-C.; Tsai, D.-S.; Fu, C.-C.; Lim, T.-S.; Tzeng, Y.-K.; Fang, C.-Y.; Han, C.-C.; *et al.* Mass Production and Dynamic Imaging of Fluorescent Nanodiamonds. *Nat. Nanotechnol.* **2008**, *3*, 284–288.
(30) Collins, A. T. The Fermi Level in Diamond. *J. Phys. Condens. Matter* **2002**, *14*, 3743–3750.
(31) Su, L.-J.; Fang, C.-Y.; Chang, Y.-T.; Chen, K.-M.; Yu, Y.-C.; Hsu, J.-H.; Chang, H.-C. Creation of High Density Ensembles of Nitrogen-Vacancy Centers in Nitrogen-Rich Type Ib Nanodiamonds. *Nanotechnology* **2013**, *24*, 315702.
(32) Rondin, L.; Dantelle, G.; Slablab, a.; Grosshans, F.; Treussart, F.; Bergonzo, P.; Perruchas, S.; Gacoin, T.; Chaigneau, M.; Chang, H.-C.; *et al.* Surface-Induced Charge State Conversion of Nitrogen-Vacancy Defects in Nanodiamonds. *Phys. Rev. B* **2010**, *82*, 1–5.
(33) Tisler, J.; Balasubramanian, G.; Naydenov, B.; Kolesov, R.; Grotz, B.; Reuter, R.; Boudou, J.-P.; Curmi, P. a.; Sennour, M.; Thorel, A.; *et al.* Fluorescence and Spin Properties of Defects in Single Digit Nanodiamonds. *ACS Nano* **2009**, *3*, 1959–1965.
(34) Botsoa, J.; Sauvage, T.; Adam, M.-P.; Desgardin, P.; Leoni, E.; Courtois, B.; Treussart, F.; Barthe, M.-F. Optimal Conditions for NV- Center Formation in Type-1b Diamond Studied Using Photoluminescence and Positron Annihilation Spectroscopies. *Phys. Rev. B* **2011**, *84*, 125209.
(35) Boudou, J.-P.; Curmi, P. A.; Jelezko, F.; Wrachtrup, J.; Aubert, P.; Sennour, M.; Balasubramanian, G.; Reuter, R.; Thorel, A.; Gaffet, E. High Yield Fabrication of Fluorescent Nanodiamonds. *Nanotechnology* **2009**, *20*, 235602.
(36) Dantelle, G.; Slablab, A.; Rondin, L.; Lainé, F.; Carrel, F.; Bergonzo, P.; Perruchas, S.; Gacoin, T.; Treussart, F.; Roch, J.-F. Efficient Production of NV Colour Centres in Nanodiamonds Using High-Energy Electron Irradiation. *J. Lumin.* **2010**, *130*, 1655–1658.
(37) Remes, Z.; Micova, J.; Krist, P.; Chvatil, D.; Effenberg, R.; Nesladek, M. N-V-Related Fluorescence of the Monoenergetic High-Energy Electron-Irradiated Diamond Nanoparticles. *Phys. status solidi* **2015**, *212*, 2519–2524.
(38) Shames, A. I.; Osipov, V. Y.; Boudou, J. P.; Panich, A. M.; von Bardeleben, H. J.; Treussart, F.; Vul', A. Y. Magnetic Resonance Tracking of Fluorescent Nanodiamond Fabrication. *J. Phys. D. Appl. Phys.* **2015**, *48*, 155302.
(39) Smith, B. R.; Inglis, D. W.; Sandnes, B.; Rabeau, J. R.; Zvyagin, A. V; Gruber, D.; Noble, C. J.; Vogel, R.; Osawa, E.; Plakhotnik, T. Five-Nanometer Diamond with Luminescent Nitrogen-Vacancy Defect Centers. *Small* **2009**, *5*, 1649–1653.
(40) Schirhagl, R.; Chang, K.; Loretz, M.; Degen, C. L. Nitrogen-Vacancy Centers in Diamond: Nanoscale Sensors for Physics and Biology. *Annu. Rev. Phys. Chem.* **2014**, *65*, 83–105.
(41) Hui, Y. Y.; Chang, H.-C. Recent Developments and Applications of Nanodiamonds as Versatile Bioimaging Agents. *J. Chinese Chem. Soc.* **2014**, *61*, 67–76.

(42) Rondin, L.; Tetienne, J.-P.; Hingant, T.; Roch, J.-F.; Maletinsky, P.; Jacques, V. Magnetometry with Nitrogen-Vacancy Defects in Diamond. *Reports Prog. Phys.* **2014**, *77*, 056503.
(43) Stursa, J.; Havlik, J.; Petrakova, V.; Gulka, M.; Ralis, J.; Zach, V.; Pulec, Z.; Stepan, V.; Zargaleh, S. A.; Ledvina, M.; *et al.* Mass Production of Fluorescent Nanodiamonds with a Narrow Emission Intensity Distribution. *Carbon N. Y.* **2016**, *96*, 812–818.
(44) Glenn, D. R.; Zhang, H.; Kasthuri, N.; Schalek, R.; Lo, P. K.; Trifonov, A. S.; Park, H.; Lichtman, J. W.; Walsworth, R. L. Correlative Light and Electron Microscopy Using Cathodoluminescence from Nanoparticles with Distinguishable Colours. *Sci. Rep.* **2012**, *2*, 865.
(45) Tizei, L. H. G.; Kociak, M. Spectrally and Spatially Resolved Cathodoluminescence of Nanodiamonds: Local Variations of the NV 0 Emission Properties. *Nanotechnology* **2012**, *23*, 175702.
(46) Kimura, E.; Sekiguchi, T.; Oikawa, H.; Niitsuma, J.; Nakayama, Y.; Suzuki, H.; Kimura, M.; Fujii, K.; Ushiki, T. Cathodoluminescence Imaging for Identifying Uptaken Fluorescence Materials in Kupffer Cells Using Scanning Electron Microscopy. *Arch. Histol. Cytol.* **2004**, *67*, 263–270.
(47) Beveratos, A.; Brouri, R.; Gacoin, T.; Poizat, J.-P.; Grangier, P. Nonclassical Radiation from Diamond Nanocrystals. *Phys. Rev. A* **2001**, *64*, 061802.
(48) Greffet, J.-J.; Hugonin, J.-P.; Besbes, M.; Lai, N. D.; Treussart, F.; Roch, J.-F.-F. Diamond Particles as Nanoantennas for Nitrogen-Vacancy Color Centers. *arXiv.org* **2011**, *Quantum ph*, 1–4.
(49) Mohtashami, A.; Femius Koenderink, A. Suitability of Nanodiamond Nitrogen–vacancy Centers for Spontaneous Emission Control Experiments. *New J. Phys.* **2013**, *15*, 043017.
(50) Faklaris, O.; Garrot, D.; Joshi, V.; Druon, F.; Boudou, J.; Sauvage, T.; Georges, P.; Curmi, P. A.; Treussart, F. Detection of Single Photoluminescent Diamond Nanoparticles in Cells and Study of the Internalization Pathway. *Small* **2008**, *4*, 2236–2239.
(51) Kuo, Y.; Hsu, T.; Wu, Y.; Chang, H.-C. Fluorescent Nanodiamond as a Probe for the Intercellular Transport of Proteins in Vivo. *Biomaterials* **2013**, *34*, 8352–8360.
(52) Wu, T.; Tzeng, Y.-K.; Chang, W.-W.; Cheng, C.-A.; Kuo, Y.; Chien, C.; Chang, H.-C.; Yu, J. Tracking the Engraftment and Regenerative Capabilities of Transplanted Lung Stem Cells Using Fluorescent Nanodiamonds. *Nat. Nanotechnol.* **2013**, *8*, 682–689.
(53) Faklaris, O.; Garrot, D.; Joshi, V.; Boudou, J.; Sauvage, T.; Curmi, P. A.; Treussart, F. Comparison of the Photoluminescence Properties of Semiconductor Quantum Dots and Non-Blinking Diamond Nanoparticles. Observation of the Diffusion of Diamond Nanoparticles in Living Cells. *J. Eur. Opt. Soc. Rapid Publ.* **2009**, *4*, 09035.
(54) Wildanger, D.; Patton, B. R.; Schill, H.; Marseglia, L.; Hadden, J. P.; Knauer, S.; Schönle, A.; Rarity, J. G.; O'Brien, J. L.; Hell, S. W.; *et al.* Solid Immersion Facilitates Fluorescence Microscopy with Nanometer Resolution and Sub-Ångström Emitter Localization. *Adv. Mater.* **2012**, *24*, OP309–OP313.
(55) Arroyo-Camejo, S.; Adam, M.-P.; Besbes, M.; Hugonin, J.-P.; Jacques, V.; Greffet, J.-J.; Roch, J.-F.; Hell, S. W.; Treussart, F. Stimulated Emission Depletion Microscopy Resolves Individual Nitrogen Vacancy Centers in Diamond Nanocrystals. *ACS Nano* **2013**, *7*, 10912–10919.
(56) Tizei, L. H. G.; Kociak, M. Spatially Resolved Quantum Nano-Optics of Single Photons Using an Electron Microscope. *Phys. Rev. Lett.* **2013**, *110*, 153604.
(57) Zaitsev, A. M. *Optical Properties of Diamond*; 1st editio.; Springer, 2001.
(58) Clark, C. D.; Kanda, H.; Kiflawi, I.; Sittas, G. Silicon Defects in Diamond. *Phys. Rev. B* **1995**, *51*, 16681–16688.
(59) Goss, J. P.; Jones, R.; Breuer, S. J.; Briddon, P. R.; Öberg, S. The Twelve-Line 1.682 eV Luminescence Center in Diamond and the Vacancy-Silicon Complex. *Phys. Rev. Lett.* **1996**, *77*, 3041–3044.
(60) Hepp, C.; Müller, T.; Waselowski, V.; Becker, J. N.; Pingault, B.; Sternschulte, H.; Steinmüller-Nethl, D.; Gali, A.; Maze, J. R.; Atatüre, M.; *et al.* Electronic Structure of the Silicon Vacancy Color Center in Diamond. *Phys. Rev. Lett.* **2014**, *112*, 036405.
(61) Rogers, L. J.; Jahnke, K. D.; Doherty, M. W.; Dietrich, A.; McGuinness, L. P.; Müller, C.; Teraji, T.; Sumiya, H.; Isoya, J.; Manson, N. B.; *et al.* Electronic Structure of the Negatively Charged Silicon-Vacancy Center in Diamond. *Phys. Rev. B* **2014**, *89*, 235101.
(62) Edmonds, A. M.; Newton, M. E.; Martineau, P. M.; Twitchen, D. J.; Williams, S. D. Electron Paramagnetic Resonance Studies of Silicon-Related Defects in Diamond. *Phys. Rev. B* **2008**, *77*, 245205.
(63) Varnin, V. P.; Laptev, V. A.; Ralchenko, V. G. The State of the Art in the Growth of Diamond Crystals and

Films. *Inorg. Mater.* **2006**, *42*, S1–S18.
(64) Zhang, H.; Aharonovich, I.; Glenn, D. R.; Schalek, R.; Magyar, A. P.; Lichtman, J. W.; Hu, E. L.; Walsworth, R. L. Silicon-Vacancy Color Centers in Nanodiamonds: Cathodoluminescence Imaging Markers in the Near Infrared. *Small* **2014**, *10*, 1908–1913.
(65) Neu, E.; Arend, C.; Gross, E.; Guldner, F.; Hepp, C.; Steinmetz, D.; Zscherpel, E.; Ghodbane, S.; Sternschulte, H.; Steinm??ller-Nethl, D.; *et al.* Narrowband Fluorescent Nanodiamonds Produced from Chemical Vapor Deposition Films. *Appl. Phys. Lett.* **2011**, *98*, 12–15.
(66) Liang, Y.; Ozawa, M.; Krueger, A. A General Procedure to Functionalize Agglomerating Nanoparticles Demonstrated on Nanodiamond. *ACS Nano* **2009**, *3*, 2288–2296.
(67) Davydov, V. A.; Rakhmanina, A. V.; Lyapin, S. G.; Ilichev, I. D.; Boldyrev, K. N.; Shiryaev, A. A.; Agafonov, V. N. Production of Nano- and Microdiamonds with Si-V and N-V Luminescent Centers at High Pressures in Systems Based on Mixtures of Hydrocarbon and Fluorocarbon Compounds. *JETP Lett.* **2014**, *99*, 585–589.
(68) Shenderova, O. A.; Vlasov, I. I.; Turner, S.; Van Tendeloo, G.; Orlinskii, S. B.; Shiryaev, A. A.; Khomich, A. A.; Sulyanov, S. N.; Jelezko, F.; Wrachtrup, J. Nitrogen Control in Nanodiamond Produced by Detonation Shock-Wave-Assisted Synthesis. *J. Phys. Chem. C* **2011**, *115*, 14014–14024.
(69) Dolmatov, V. Y.; Kulakova, I. I.; Myllymäki, V.; Vehanen, A.; Panova, A. N.; Voznyakovskii, A. A. IR Spectra of Detonation Nanodiamonds Modified during the Synthesis. *J. Superhard Mater.* **2014**, *36*, 344–357.
(70) Barnard, A. S.; Sternberg, M. Substitutional Nitrogen in Nanodiamond and Bucky-Diamond Particles. *J. Phys. Chem. B* **2005**, *109*, 17107–17112.
(71) Vlasov, I. I.; Barnard, A. S.; Ralchenko, V. G.; Lebedev, O. I.; Kanzyuba, M. V.; Saveliev, A. V.; Konov, V. I.; Goovaerts, E. Nanodiamond Photoemitters Based on Strong Narrow-Band Luminescence from Silicon-Vacancy Defects. *Adv. Mater.* **2009**, *21*, 808–812.
(72) Barnard, A. S.; Vlasov, I. I.; Ralchenko, V. G. Predicting the Distribution and Stability of Photoactive Defect Centers in Nanodiamond Biomarkers. *J. Mater. Chem.* **2009**, *19*, 360–365.
(73) Vlasov, I. I.; Shiryaev, A. A.; Rendler, T.; Steinert, S.; Lee, S.; Antonov, D.; Vörös, M.; Jelezko, F.; Fisenko, A. V; Semjonova, L. F.; *et al.* Molecular-Sized Fluorescent Nanodiamonds. *Nat. Nanotechnol.* **2013**, *9*, 54–58.
(74) Bradac, C.; Gaebel, T.; Pakes, C. I.; Say, J. M.; Zvyagin, A. V; Rabeau, J. R. Effect of the Nanodiamond Host on a Nitrogen-Vacancy Color-Centre Emission State. *Small* **2013**, *9*, 132–139.
(75) Shershulin, V. A.; Sedov, V. S.; Ermakova, A.; Jantzen, U.; Rogers, L.; Huhlina, A. A.; Teverovskaya, E. G.; Ralchenko, V. G.; Jelezko, F.; Vlasov, I. I. Size-Dependent Luminescence of Color Centers in Composite Nanodiamonds. *Phys. status solidi* **2015**, *212*, 2600–2605.
(76) Merson, T. D.; Castelletto, S.; Aharonovich, I.; Turbic, A.; Kilpatrick, T. J.; Turnley, A. M. Nanodiamonds with Silicon Vacancy Defects for Nontoxic Photostable Fluorescent Labeling of Neural Precursor Cells. *Opt. Lett.* **2013**, *38*, 4170.
(77) Tizei, L. H. G.; Meuret, S.; Nagarajan, S.; Treussart, F.; Fang, C.-Y.; Chang, H.-C.; Kociak, M. Spatially and Spectrally Resolved Cathodoluminescence with Fast Electrons: A Tool for Background Subtraction in Luminescence Intensity Second-Order Correlation Measurements Applied to Subwavelength Inhomogeneous Diamond Nanocrystals. *Phys. status solidi* **2013**, *210*, 2060–2065.

***